Activation of Notch signalling by soluble Dll4 decreases vascular permeability via a cAMP/PKA-dependent pathway

[1]Rachel Boardman, [1]Vincent Pang, [1]Naseeb Malhi, [1]Amy P Lynch, [2]Lopa Leach, [1,3]Andrew V Benest, *[1,3]David O Bates, [1]Maria J C Machado

[1]Cancer Biology, Division of Cancer and Stem Cells, School of Medicine, Queen's Medical Centre, D Floor, West Block, University of Nottingham, Nottingham NG7 2UH

[2]Division of Physiology Pharmacology and Neuroscience, School of Life Sciences, The Medical School, Nottingham NG7 2UH

[3]COMPARE University of Birmingham and University of Nottingham Midlands

*Author for correspondence David.Bates@nottingham.ac.uk

ABSTRACT

The Notch ligand Delta-like ligand 4 (Dll4), upregulated by Vascular Endothelial Growth Factor (VEGF), is a key regulator of vessel morphogenesis and function, controlling tip and stalk cell selection during sprouting angiogenesis. Inhibition of Dll4 results in hyper-sprouting, non-functional, poorly perfused vessels, suggesting a role for Dll4 in formation of mature, reactive, functional vessels, with low permeability and able to restrict fluid and solute exchange. We tested the hypothesis that Dll4 controls transvascular fluid exchange. A recombinant protein expressing only the extracellular portion of Dll4 (soluble Dll4: sDll4) induced Notch signalling in endothelial cells (EC), resulting in increased expression of VE-Cadherin, but not the tight junctional protein ZO1, at intercellular junctions. sDll4 decreased permeability of fluorescein isothiocyanate (FITC)-labelled albumin across EC monolayers and this effect was abrogated by co-culture with the γ-secretase inhibitor DAPT. One of the known molecular effectors responsible for strengthening EC-EC contacts is the cyclic AMP-dependent protein kinase A (PKA), so we tested the effect of modulation of PKA on sDll4-mediated reduction of permeability. Inhibition of PKA reversed the sDll4-mediated reduction in permeability and reduced expression of the Notch target gene Hey-1. Knockdown of PKA reduced the sDLL4 mediated VE-cadherin junctional expression. sDll4 also caused a significant decrease in the hydraulic conductivity of rat mesenteric microvessels *in vivo*. This reduction was abolished upon co-perfusion with the PKA inhibitor H89 dihydrochloride. These results indicate that Dll4 signalling through Notch activation acts through a cAMP/PKA pathway upon intercellular adherens junctions, but not tight junctions, to regulate endothelial barrier function.

INTRODUCTION

In mature and quiescent functional vascular networks, the vessel wall forms a semi-permeable barrier, which regulates the exchange of fluid and solutes between the blood and tissues. Vascular permeability is also tightly controlled during physiological angiogenesis, in development, the female reproductive cycle and wound healing (6). Dysregulated vessel permeability is a symptom of pathologies such as cancer, diabetes and cardiovascular disease, where it results in oedema, facilitation of metastatic spread, vision loss, proteinuria and kidney failure (15, 18, 30)

Vascular Endothelial Growth Factor (VEGF) is the principal mediator of the angiogenic switch and a potent inducer of vessel permeability (5, 7, 25, 40) and, as such, therapies targeting VEGF were developed to reduce permeability back to pre-pathological levels (38) (44). Administration of anti-VEGF antibodies succeeded in reducing permeability in pre-clinical trials in cancer and retinal disease (26, 28), and clinical trials have demonstrated that anti-VEGF antibodies reduce oedema in the retina, in a substantial proportion of patients, but not all (12). This suggests that regulation of permeability during angiogenesis has multiple components (22). As a result, the therapeutic potential of other molecules, and especially those that act through lateral inhibition such as Delta-like ligand 4 (Dll4), has started to be explored (31).

Dll4 is over-expressed in tumour vasculature (32) and, in tumour-bearing animals. The use of a neutralising antibody has led to an inhibition of tumour growth (37), which was shown to be a consequence of non-productive

angiogenesis (31). Tumours treated with Dll4 inhibitors exhibited reduced pericyte coverage, increased vascular leakage and impaired vascular integrity (13) (24), which supported the rationale behind Dll4-targeted therapies for cancer treatment. It also hinted at a role for Dll4 in the maintenance of endothelial barrier integrity. More recently, targeting of delta-like 1 homologue, a tumour pericyte-associated antigen and Notch antagonist, has led to the development of combined vaccination approaches that lead to reduced vascular permeability and vascular normalization (11) (16). We therefore tested the hypothesis that Dll4 could control permeability of endothelial barriers *in vitro* and *in vivo*.

77 METHODS

78

79 **Cells, recombinant proteins and inhibitors**

80 Human dermal blood endothelial cells (HDBECs) were purchased from
81 Promocell, cultured in EBM-2 complete media (Lonza) and maintained at
82 37°C in a humidified chamber with 5% CO_2. HUVECS were cultured and
83 expanded in Endothelial Cell Basal Medium (PromoCell GmbH, Heidelberg,
84 Germany).

85

86 Recombinant human VEGF-A_{165}a (40ng/mL), recombinant human sDll4 (aa
87 27-524; 1µg/mL), the γ-secretase inhibitor N-[N-(3,5-Difluorophenacetyl)-L-
88 alanyl]-S-phenylglycine t-butyl ester (DAPT, Tocris BioScience), and *N*-[2-[[3-
89 (4-Bromophenyl)-2-propenyl]amino]ethyl]-5-isoquinolinesulfonamide
90 dihydrochloride (H89), a PKA inhibitor (Tocris BioScience; 1µM) were used to
91 both treat HDBECs or to perfuse mesenteric vessels *in vivo*. For knockdown
92 experiments, 24 h prior to transfection HUVECs were seeded at 20,000
93 cells/cm^2. For immunofluorescence, cells were cultured on coverslips coated
94 with 0.2 % gelatin in PBS (Sigma Aldrich). Four different PKA siRNA (1-4,
95 Table 1, Sigma-Aldrich) or scrambled siRNA were transfected using
96 Oligofectamine (Invitrogen) at a final concentration of 200 nM in 100 µL
97 OptiMEM (Gibco) as per manufacturers instructions.

98

99 **Quantitative RT-PCR**

100 RNA extraction was performed with TRI reagent (Sigma) and cDNA was
101 generated using the Takara Prime script RT kit. Pre-validated primers for
102 human genes Hairy/enhancer-of-split related with YRPW motif protein 1

(HES1, HEY1) and Glyceraldehyde 3-phosphate dehydrogenase (GAPDH) were purchased from Qiagen. Human β-Actin primers and human PKA primers were used as in Table 2. PCR reactions were performed in triplicate with 10µl Lightcycler 480 SYBR Green 1 mastermix (Roche), 2µl primer sets, 2µl cDNA and 8µl water. Expression relative to control was calculated from the cycle thresholds (CT) and calculated as the difference between the test CT and the housekeeping gene (ΔCT) subtracted from the mean control sample ΔCT (ΔΔCT) and assuming doubling efficiency of 1 ($2^{-\Delta\Delta CT}$).

Transwell assay

Corning transwell inserts (6.5mm diameter, 0.4µm pore size) coated with 1% gelatin solution were used to seed HDBECs at a density of 5 x 10^4 cells/insert. Relative media volumes were 100µL in the insert and 600µL in the lower compartment to avoid changes in hydrostatic pressure. Once cells had become confluent, a FITC-Bovine Serum Albumin (BSA) solution (1mg/mL) was added to both compartments and treatments started after 30 minutes of equilibration. Samples of phenol-free media were taken from both compartments at 30 minute intervals and their absorbance read at 492/520nm absorption/emission.

Immunofluorescence, staining and imaging

Sterile 13mm^2 coverslips coated with 0.2mg/cm^2 fibronectin were used to plate 3 x 10^4 HDBECs, or 0.2% gelatin for HUVECs. The cells were incubated until a monolayer was formed and then treated for 4 hours with vehicle, VEGF or sDll4. The media was then discarded and the cells were fixed in ice-cold ethanol at -20°C for 30 minutes, washed in PBS and incubated at 4°C

overnight with rabbit polyclonal anti-activated Notch1 antibody (ab8925, Abcam; 1:200), polyclonal rabbit anti-VE Cadherin antibody (ab33168, Abcam; 5µg/ml) or polyclonal rabbit anti-ZO-1 antibody (ab59720, Abcam; 10µg/ml). The following day, cells were washed and stained with donkey anti-rabbit Alexa Fluor 555-conjugated antibody (Life Technologies; 1µg/ml) and phalloidin Alexa Fluor 488-conjugated (Life Technologies; 1:500). Nuclei were stained with DAPI and the coverslips were mounted onto microscope slides with anti-fade Vectashield. z-stack images of 5 regions from each coverslip were acquired with a confocal microscope at 40x magnification. Analysis was undertaken blinded using Image J analysis software.

All *in vitro* experiments were performed in triplicate and repeated 3 times unless otherwise stated and the data are presented as mean ±SEM with the number of experimental independent replicates being the n number given and used for statistical analysis. Post-hoc power analysis indicates that all significant differences were achieved with a power greater than 80%. Power for non significant differences is given where stated. Power was calculated using G Power. The percentage of thick and thin junctions and junctional gaps was statistically analysed using a two-way ANOVA with a Bonferroni post-test and fluorescence intensity for both VE-Cadherin and ZO-1 staining was statistically analysed using a one-way ANOVA with a Bonferroni post-test. Both analyses used confidence intervals of 95%.

Measurement of hydraulic conductivity (L_p)

All animal experiments were conducted according to the Animal (Scientific Procedures) Act of 1986, according to UK legislation, and conducted in named establishments, under the authority of the Home Office.

Male Han Wistar rats (n=5 per group) were anaesthetized with 2% isoflurane vaporized in 100% O_2 and a laparotomy was performed under sterile conditions. The mesentery was draped over a quartz pillar bathed in warmed mammalian Ringer's solution and the animal moved to the imaging rig. A refillable glass micropipette was then used to cannulate a post-capillary venule and the vessel was continuously perfused with a solution of 1% bovine serum albumin (BSA, Sigma) in Ringer's solution (pH=7.40). Washed red blood cells (RBCs) were used as flow markers and the vessel was occluded at 15-20 second intervals. After approximately 8 min, the pipette was refilled again with either the control BSA solution, sDll4 or the PKA inhibitor H89 dihydrochloride (H89) and repeated occlusion of the vessel was continued. At the end of the experiment the animal was killed by cervical dislocation while still under anaesthesia. Video recordings of each vessel were analysed to calculate L_p. During each vessel occlusion, we measured the vessel radius, the distance between the occlusion site and a single RBC, and calculated its velocity; with this information, we calculated the transcapillary water flow per unit area (J_v/S), as previously described (39). Hydraulic conductivity (L_p) was then calculated as the slope of the relation between J_v/S and pressure. An unpaired t test was performed using the fold change compared to baseline maximal responses for BSA versus sDll4. A one-way ANOVA (with a Bonferroni post-test) was performed for comparison of maximal responses for sDll4 versus H89 and H89 + sDll4. Confidence levels were set at 95% and all data is presented as mean ±SEM.

178 RESULTS

179

180 **Soluble Delta-like ligand 4 (sDll4) activates Notch signalling in ECs**

181 To determine whether we could experimentally induce Dll4 forward signalling
182 we used recombinant soluble Dll4 protein. In confluent cultured endothelial
183 cells (ECs), Notch staining was diffuse and more abundant in the cytoplasm
184 (Fig 1A), whereas treatment with either 1µg/ml sDll4 or 40ng/ml VEGF-A led
185 to the appearance of punctate staining of Notch, indicating proteolytic
186 cleavage of Notch to result in the release of Notch Intracellular Domain
187 (NICD, fig 1A). Moreover, in cells treated with 1µg/ml sDll4, Notch staining
188 tended to be localized inside the nucleus (see side projection in Fig 1B).
189 To ascertain whether increased NICD translocation translates to induction of
190 the translation of target genes, we compared levels of expression of Notch
191 target genes Hes1 and Hey1. HDBECs were incubated until 80% confluent
192 and then treated for 4 hours with vehicle (negative control), VEGF (positive
193 control) or sDll4. Treatment of HDBECs with 1µg/ml sDll4 recombinant protein
194 upregulates both Hes1 (Fig 1B) and Hey1 transcripts (Fig 1C), when
195 compared with untreated cells, and at a level similar to that elicited by VEGF
196 stimulation. Although this upregulation was more pronounced for Hey1
197 (around 10-fold increase compared with untreated, Fig 1C) than for Hes1
198 (around 2-fold increase compared with untreated, Fig 1B), it was completely
199 abrogated by treatment with the γ-secretase inhibitor DAPT, both for Hes1
200 and Hey1 (Fig 1B&C), indicating that sDll4-mediated signalling acts in a
201 manner similar to the canonical understanding of Dll4-Notch1 signalling.

202

203 **sDll4 promotes endothelial junctional protein expression**

To investigate the effects of Dll4-Notch signalling on vascular permeability we first investigated changes in junctional proteins. We treated EC monolayers with VEGF or sDll4 and stained the cells with phalloidin for cytoskeletal protein F-actin and VE-Cadherin for adherens junctions (Fig 2A) or ZO-1 for tight junctions (Fig 2B). sDll4 treatment led to a rearrangement of actin fibres in cultured ECs, which were located around the periphery of the cells compared with the parallel arrangement seen in untreated and VEGF-treated cells (Fig 2A). VE-Cadherin staining tended to be localized at EC-EC junctions in untreated cells (Fig 2A). Similarly, ZO-1 expression was enhanced by sDll4, but reduced by VEGF-A (Fig 2B). The VE-Cadherin positive junctions could be divided into a thick and thin morphology (Fig 2C). In untreated cells, the VE-Cadherin positive thin junctions formed the majority (54.5%) and the thick junctions account for only 20.9% of the total junctional length. Whereas VEGF caused no significant difference in the distributions of the types of adherens junctions compared to untreated cells, sDll4 significantly decreased the percentage of thin junctions and significantly increased the percentage of thick junctions (Fig 2C). VEGF treatment also resulted in the lowest number of ZO-1-positive junctions per cell (Fig 2D). Together, these results indicate that sDll4 leads to a rearrangement of the proteins comprising adherens junctions that could result in an improvement in the barrier function of EC monolayers.

sDll4 improves endothelial barrier function *in vitro*

Having established that sDll4 induced Notch signalling in a manner similar to VEGF, and that it could affect barrier protein expression in a manner opposite to VEGF, we assessed the effect of sDll4 on permeability of confluent cells. We used a transwell assay to measure the movement of FITC-labelled

albumin across a monolayer of ECs (Fig 3). Treatment of cells with 40ng/ml VEGF-A resulted in an increase in FITC-BSA in the lower well (Fig 3A). In contrast, 1µg/ml sDll4 reduced the FITC-BSA in the lower wells compared with control. We calculated the permeability of the monolayer, assuming negligible active transport or convection, based on the solute flux (mass of FITC-BSA that crossed the transwell per 30 minute time period), the area of the membrane and the concentration gradient at that time point. Fig 3B shows that sDll4 resulted in a transient decrease in permeability at 30 minutes compared with control. VEGF-A resulted in the characteristic biphasic increase in permeability. To determine whether the reduction in permeability by Dll4 was induced through Notch, we treated the cells with the γ-secretase inhibitor DAPT for 30 minutes prior to addition of the recombinant proteins to the media. This reversed the decrease in FITC-BSA transport (Fig 3C) and the decrease in permeability (Fig 3D).

Mechanisms underlying decreased permeability are not well described. The most extensive literature on reduced permeability concerns the involvement of PKA signalling through cyclic adenosine monophosphate (cAMP) (1). We therefore investigated whether the PKA inhibitor H89 could reverse the decrease in permeability in HDBEC monolayers. Treatment of cells with 10µM H89 resulted in a significant increase in FITC-BSA in the lower well above vehicle control (Fig 3E). Treatment with sDll4 did not reduce the BSA-FITC concentration below control in the presence of H89, and after one hour there was more, not less FITC-BSA in the sDll4 treated wells than in the vehicle control. Calculation of permeability (Fig 3F) shows that the H89 baseline value was higher, and sDll4 did not reduce permeability in the presence of H89.

PKA inhibition impairs Notch signalling

Dll4-Notch has not previously been shown to signal through PKA. Therefore, to determine whether downstream transcriptional activation of Notch target genes could be abrogated by treatment with H89, we measured Hey expression. We co-treated HDBEC with VEGF-A and DAPT or sDll4 and DAPT and obtained results similar to those reported earlier (Fig 1). Figure 3G also shows that when HDBEC are co-treated with DAPT or H89 (concomitantly with VEGF-A or sDll4), they showed reduced Hey1 expression compared to vehicle. To confirm that PKA inhibition was behind the sDLL4 mediated alteration in barrier function, HUVECs were transfected with four different PKA siRNA, or a combination of all four siRNA and cells stained for junctional proteins. All four siRNAs resulted in reduced expression of PKA, and combining all four resulted in a highly significant 77.1±1.6% reduction in RNA expression (Figure 4A). The DLL4 mediated increase in thick (fig 4B) and decrease in thin (figure 4C) junctions was blocked by PKA knockdown. PKA knockdown by itself also increased the number of gaps in the VE-Cadherin stained junctions, but DLL4 again had no effect (Fig 4D). Interestingly, ZO1 staining was increased by PKA knockdown (fig 4E). These results confirm that activation of Notch signalling, both for its target genes and adherens junctional integrity, requires intact cAMP/PKA signalling.

sDll4 reduces permeability to water *in vivo*

To ascertain whether Dll4-Notch signalling resulted in a decrease in vascular permeability *in vivo*, we measured the effect of sDll4 on individually perfused microvessels of the intact rat mesentery. We used an intravital perfusion and microscopy system to cannulate and perfuse post-capillary venules in the

mesentery of anaesthetised rats. This enabled control of the oncotic and hydrostatic pressure gradients, expose cells to shear stress and rely on intact cell signalling. We used the Landis-Michel technique to measure hydraulic conductivity (Lp), where RBCs are used as flow markers (Fig 5). Control experiments showed that refilling of the cannulation pipette with 1% BSA solution did not change hydraulic conductivity (Fig 5A). In contrast, within 2 minutes of perfusion with sDll4, Lp consistently began to fall below baseline, plateauing at a minimal value after 5 minutes, where it remained until the end of the experiment (~10 minutes, Fig 5B).

sDll4-mediated decrease in Lp acts via cAMP/PKA

To understand whether the mechanism underlying the reduction in permeability affected by sDll4 also depended on PKA, we perfused mesenteric post-capillary venules with H89. This led to a slight but not statistically significant increase in the hydraulic conductivity of these vessels (Fig 5C). When sDll4 and H89 were perfused together, Lp changed in a manner similar to H89 perfusion (Fig 5D), not sDll4, making the difference in Lp a very significant increase compared to sDll4 alone (Fig 5E). These results clearly demonstrate that, *in vivo*, sDll4 is acting through a cAMP/PKA dependent pathway to regulate microvessel permeability.

DISCUSSION

The upregulation of the Notch ligand, Dll4 (27) is a downstream consequence of VEGF signalling through VEGF receptor 2 (VEGFR2). The subsequent paracrine reciprocal interaction of Dll4 with Notch has been recognized as the principal molecular mechanism giving rise to the tip or stalk cell phenotypes in sprouting angiogenesis (20) (41). Dll4 will bind to Notch on an adjacent EC membrane, leading to the γ-secretase mediated proteolytic cleavage of Notch and the subsequent release of the Notch Intracellular Domain (NICD) (10). The NICD translocates to the nucleus where it interacts with recombination signal binding protein for immunoglobulin kappa J region (RBPJ-κ). Upon binding, allosteric changes occur in RBPJ-κ which enable the displacement of transcriptional repressors and the subsequent transcription of Notch target genes such as Hes1 and Hey1 (19). Dll4/Notch signalling then negatively regulates VEGFR2 expression (41) with Notch playing an essential part in vascular plexus remodelling and maturation (14). To validate our experimental approach, we compared the effect of VEGF with the extracellular portion of Dll4 (sDll4) and found that sDll4 is sufficient to activate Notch signalling (Fig 1).

During sprouting angiogenesis, VE-Cadherin, the principal component of endothelial adherens junctions, is expressed on the anterior plasma membrane and in filopodia protrusions of tip cells (3). However, the continual flux in Notch levels in individual EC results in differential VE-cadherin turnover and junctional-cortex protrusions (8), which powers differential cell movement when EC compete for the tip cell position, first described in embryoid bodies (21). Thus, Dll4/Notch signalling at EC-EC junctions seems to play an

329 essential role in maintaining endothelial barrier integrity, especially during
330 angiogenesis. Inhibition of γ-secretase with DAPT leads to inhibition of
331 Dll4/Notch signalling (Fig 1) but it also has effects on other transmembrane
332 proteins. In breast cancer cells, DAPT blocks E-cadherin cleavage (46). In
333 cultured hippocampal neurons, endoplasmic reticulum loss was inhibited by
334 DAPT, and this correlates with proteolytic activity affecting adherens junctions
335 (29). In a rat model of permanent middle cerebral artery occlusion, DAPT
336 reduced the permeability of the blood brain barrier by decreasing the
337 ubiquitination and degradation of occludin (47). However, when we tested the
338 effect of sDll4 in confluent cultured endothelial cells, we found that sDll4-
339 treated ECs undergo a change in expression and distribution of proteins that
340 constitute adherens junctions, but not those involved in tight junctions (Fig 2),
341 and reduces permeability in intact quiescent blood vessels. This suggests that
342 previously described reduction in permeability by inhibition of the Notch
343 pathway may be context dependent (active or confluent ECs) and tissue
344 dependent (blood brain barrier compared with systemic capillaries).
345 cAMP has been shown to stabilise the endothelial barrier by reducing myosin
346 light chain phosphorylation (45) (9), inhibiting the GTPase RhoA (34),
347 preventing Rac1 inhibition (43) and acting through Epac/Rap1 to stabilise
348 cortical actin (2), leading to an increase in cytoskeletal-associated VE-
349 Cadherin. Here, we add to this knowledge by showing that sDll4 decreases
350 solute flux across an endothelial cell monolayer and this is reversed by H89,
351 an inhibitor of PKA (Fig 3), and that this PKA mediated re-arrangement
352 controls adherens junctional formation (but not tight junctional components
353 such as ZO1). This indicates that PKA-dependent cAMP signalling mediates

DLL4 mediated VE-Cadherin assembly at adherens junctions and promotes endothelial barrier integrity.

Recently, the link between VE-Cadherin and Dll4/Notch signalling has been further explored (33). Using an engineered blood vessel model, the authors found that a novel LAR/Trio/Rac1 complex is formed due to Notch “non-canonical” signalling to drive assembly of adherens junctions, in response to shear stress. Rac1 has been shown to be downstream of cAMP, in thrombin induced permeability enhancement in ECs (4). In the present paper, we further add to the mechanistic insight into Dll4/Notch mediated reduction in permeability, finding that this non-canonical signalling is through cAMP-mediated activation of PKA, which causes a reduction in barrier function, presumably through phosphorylation of Rac1, allowing it to facilitate the interaction between the Lar-Notch1 TMD-VE-Cadherin complex through the GEF-Trio axis (Fig 6). Further we show here that this results in an actual decrease in permeability of the barrier wall *in vivo* (Fig 5), rather than just a reduction in solute flux, which could be explained by haemodynamic changes.

Over the years, a number of papers have linked the formation of mechanosensing complexes with endothelial barrier function (42) (17). What was once thought of as arterial specification during development may be mechanistically linked to sensing of shear stress (23). Indeed, low shear stress-induced atherosclerotic plaque formation was inhibited by DAPT, with the subsequent downregulation of NICD and ICAM-1 (35). This may not be limited to ECs, since pericyte-derived Dll4 may control involution of infantile haemangioma in a VEGF-independent manner (23). Of interest was the distinguishment of tight junctional protein rearrangement from adherens junctions (figs 2 and 4). Whereas sDLL4 did not affect ZO1 expression, PKA

knockdown increased it, which was blocked by sDLL4. This indicates that there are two different mechanisms for regulating permeability through the two different pathways. This could be due to localization of PKA to the different junctional compartments, a mechanism proposed by Radeva et al to be mediated by AKAP12(36).

In summary, we show here for the first time that Dll4 mediated activation of Notch can reduce hydraulic conductivity, and hence the permeability of the capillary wall, through activation of cAMP. This supports the concept that fluid and solute exchange is limited in normal vasculature by Notch signalling through regulation of adherens junctions.

ACKNOWLEDGEMENTS

This work was supported by the Medical Research Council (MR/K013157/1 and 1361718), the British Heart Foundation (PG/13/85/30536, PG/18/31/33759) and the National Eye Research Centre

Author Contributions.

Conception and design DOB, MJCM, AVB, LL; organisation of the conduct DOB, MJCM, AVB, LL; carrying out experiments, RB, AVB, NM, AL, VP ; analysis and interpretation of the study data DOB, MJCM, AVB, RB, NM, VP. All authors helped draft and critique the output for important intellectual content.

FIGURE LEGENDS

Figure 1: sDll4 promotes Notch intracellular signalling in endothelial cells. A) Representative confocal images of HDBECs which were treated with VEGF, sDll4 or vehicle control and then stained for Notch 1 (red) and phalloidin (green) with nuclear counterstain for Hoechst (blue) reveal nuclear localization and punctate staining of Notch 1 upon VEGF or sDll4 treatment. **B**. Z projection of cells demonstrating nuclear (blue arrow) expression of Notch 1 (red arrow) in sDLL4 and VEGF treated cells, but not in vehicle treated cells. Scale bar=25μm. VEGF and sDll4 treatment result in indistinguishable increase in the expression of Notch 1 target genes **C)** Hes 1 and **D)** Hey 1 relative to vehicle, as assessed by ddPCR; this upregulation in RNA transcription is impaired by co-treatment of HDBECs with DAPT.

Figure 2: sDll4 promotes the re-arrangement of adherens junctions. Representative confocal images of HDBECs which were treated with VEGF, sDll4 or vehicle control and then stained for phalloidin (green) and **A)** VE-Cadherin for adherens junctions (red) or **B)** ZO-1 for tight junctions (red) with nuclear counterstain for DAPI (blue). Scale bar=25μm. Image analysis was performed using FIJI to quantify **C)** the percentage of intercellular space occupied by gaps or VE-Cadherin-positive intercellular junctions between cells and **D)** the number of ZO-1-positive junctions per cell. VEGF treatment led to an increase in the number of gaps and decrease in the number of junctions per cell, whilst sDll4 promoted the formation of thicker adherens junctions. **p<0.01; ***p<0.005; ****p<0.001, two-way ANOVA with 95% CI and Bonferroni post-test.

Figure 3: sDll4 decreases endothelial monolayer permeability via cAMP. **A)** In EC monolayers, the flux of FITC-labelled BSA reaches 4μg/mL after 2 hours (N=6), whereas, in the presence of $VEGF_{165}a$, it increases to over 10μg/mL (N=8). sDll4 decreases FITC concentration to below that of vehicle, and significantly below VEGF (N=8). **B)** This translates in a typical biphasic response for VEGF permeability, that is counter-acted in a mirroring behaviour by the effect of sDll4 on the EC monolayer. **C)** Inhibition of sDll4 (N=5) with DAPT (N=5) increases FITC concentration and **D)** permeability above vehicle. **E)** PKA inhibition with H89 resulted in increased permeability above vehicle (N=3), which was not impaired by sDll4 (N=3); in effect, **F)** permeability was the same for H89 and sDll4+H89. **G)** Both DAPT and H89 were able to abolish both VEGF and sDll4-mediated increases in Hey1 gene expression (N=3 per group). P<0.001 ANOVA with Bonferroni post-test. ***=p<0.001 compared with vehicle. #=p<0.05 compared with DAPT, ++=p<0.01 compared with H89. ANOVA with Bonferroni post-test.

Figure 4. Formation of adherens junctions by DLL4 is PKA dependent. **A)** Knockdown of PKA using four different PKA siRNAs. Cells were treated with the siRNA and RNA extracted and amplified by Q-PCR after 48 hours. N=3 HUVECs were stained for VE-Cadherin and ZO-1 and junctional type calculated as in figure 2. The increase in thick junctions (**B**) and decrease in thin junctions (**C**) was blocked by PKA knockdown. PKA knockdown increased the percentage of gaps (**D**), in the absence but not the presence of sDLL4. **E)** ZO1 junctional staining was increased by PKA knockdown in the absence but not the presence of sDLL4. *=p<0.01, **=p<0.01, ***=p<0.001

compared with scrambled control. ##=p<0.01 compared with sDLL4. B-E, N=5 ANOVA with Bonferroni post-test.

Figure 5: sDll4 decreases hydraulic conductivity *in vivo* via a cAMP/PKA-dependent pathway. Calculation of hydraulic conductivity (Lp) in post-capillary venules of the mesentery of rats revealed that **A)** reperfusion with BSA does not alter vascular permeability (N=5). **B**) Perfusion with sDll4 showed a clear decrease in permeability compared to BSA within 120 seconds until it plateaued at 300 seconds (N=5). Whilst **C)** H89 perfusion had no effect in water permeability relative to BSA baseline (N=5), **D)** perfusion with the combination of H89 and sDll4 did not result in a change in Lp despite constant fluctuations around baseline (N=5). **E)** Relative to BSA vehicle, peak response in sDll4 gave rise to around 60% decrease in water permeability, which was completely abrogated by H89. P<0.001 ANOVA with Bonferroni post-test. ***=p<0.001 compared with BSA. +++=p<0.001 compared with DLL4+H89

Figure 6. Schematic for the junctional regulation of VE-Cadherin by Dll4-Notch signalling. The endothelial cells, covered by a layer of glycocalyx, forms an intercellular cleft where two endothelial cells meet. The cleft contains adherens junctions, and tight junctions (not shown). The AJ consist of VE-Cadherin bound to multiple signalling molecules (not shown). Upon activation of Notch by Dll4, cAMP is generated, either directly or indirectly, which results in strengthening of the VE-Cadherin junctions. Recent work by Polacheck et al has shown that the transmembrane domain of Notch can bind to Lar-Trio-Rac1 complex, which is known to be activated by phosphorylation by PKA.

482

483 Table 1. siRNA sequences.

siRNA	SEQUENCE 5'-3'
PKA1F	GAACACACCCUGAAUGAAAUU
PKA1F AS	UUUCAUUCAGGGUGUGUUCUU
PKA2F	GAACACAGCCCACUUGGAUUU
PKA2FAS	AUCCAAGUGGGCUGUGUUCUU
PKFA3F	CAAGGACAACUCAAACUUAUU
PKFA3FAS	UAAGUUUGAGUUGUCCUUGUU
PKFA4	GCUAAGGGCAAAUGAACGAUU
PKA4FAS	UCGUUCAUUUGCCCUUAGCUU

484

485 Table 2. Primer sequences and sources

Primer	Source	Sequence	Catalogue number
Hes 1.	Qiagen	Not disclosed by supplier	QT00039648
Hey 1.	Qiagen	Not disclosed by supplier	QT00035644
GAPDH	Qiagen	Not disclosed by supplier	QT00079247
Actin fwd	Qiagen	5'CCCAGCACAATGAAGATCAA3'	
Actin rev	Qiagen	5'CGATCCACACGGAGTACTTG3'	
PKA fwd	Qiagen	5'GAAGATCGTCTCTGGGAAGT3'	
PKA rev	Qiagen	5'TGACCCCATTCTTGAGGTTC3'	

486

487

References

1. **Adamson RH, Liu B, Fry GN, Rubin LL, and Curry FE**. Microvascular permeability and number of tight junctions are modulated by cAMP. *Am J Physiol* 274: H1885-1894., 1998.
2. **Adamson RH, Ly JC, Sarai RK, Lenz JF, Altangerel A, Drenckhahn D, and Curry FE**. Epac/Rap1 pathway regulates microvascular hyperpermeability induced by PAF in rat mesentery. *Am J Physiol Heart & Circ* 294: H1188-1196, 2008.
3. **Almagro S, Durmort C, Chervin-Petinot A, Heyraud S, Dubois M, Lambert O, Maillefaud C, Hewat E, Schaal JP, Huber P, and Gulino-Debrac D**. The motor protein myosin-X transports VE-cadherin along filopodia to allow the formation of early endothelial cell-cell contacts. *Mol Cell Biol* 30: 1703-1717, 2010.
4. **Aslam M, Tanislav C, Troidl C, Schulz R, Hamm C, and Gunduz D**. cAMP controls the restoration of endothelial barrier function after thrombin-induced hyperpermeability via Rac1 activation. *Physiol Rep* 2: 2014.
5. **Bates DO**. Chronically increased hydraulic conductivity (Lp) by vascular endothelial growth factor (VEGF) is attenuated by inhibition of calcium influx. *J Physiol (Lond)* in press: 2001.
6. **Bates DO**. Vascular endothelial growth factors and vascular permeability. *Cardiovasc Res* 87: 262-271, 2010.
7. **Bates DO, and Curry FE**. Vascular endothelial growth factor increases hydraulic conductivity of isolated perfused microvessels. *American Journal of Physiology: Heart and Circulatory Physiology* 271: H2520-H2528, 1996.
8. **Bentley K, Franco CA, Philippides A, Blanco R, Dierkes M, Gebala V, Stanchi F, Jones M, Aspalter IM, Cagna G, Westrom S, Claesson-Welsh L, Vestweber D, and Gerhardt H**. The role of differential VE-cadherin dynamics in cell rearrangement during angiogenesis. *Nat Cell Biol* 16: 309-321, 2014.
9. **Bindewald K, Gunduz D, Hartel F, Peters SC, Rodewald C, Nau S, Schafer M, Neumann J, Piper HM, and Noll T**. Opposite effect of cAMP signaling in endothelial barriers of different origin. *Am J Physiol Cell Physiol* 287: C1246-1255, 2004.
10. **Caolo V, van den Akker NM, Verbruggen S, Donners MM, Swennen G, Schulten H, Waltenberger J, Post MJ, and Molin DG**. Feed-forward signaling by membrane-bound ligand receptor circuit: the case of NOTCH DELTA-like 4 ligand in endothelial cells. *J Biol Chem* 285: 40681-40689, 2010.
11. **Chi Sabins N, Taylor JL, Fabian KP, Appleman LJ, Maranchie JK, Stolz DB, and Storkus WJ**. DLK1: a novel target for immunotherapeutic remodeling of the tumor blood vasculature. *Mol Ther* 21: 1958-1968, 2013.
12. **Diabetic Retinopathy Clinical Research N, Wells JA, Glassman AR, Ayala AR, Jampol LM, Aiello LP, Antoszyk AN, Arnold-Bush B, Baker CW, Bressler NM, Browning DJ, Elman MJ, Ferris FL, Friedman SM, Melia M, Pieramici DJ, Sun JK, and Beck RW**. Aflibercept, bevacizumab, or ranibizumab for diabetic macular edema. *N Engl J Med* 372: 1193-1203, 2015.
13. **Djokovic D, Trindade A, Gigante J, Badenes M, Silva L, Liu R, Li X, Gong M, Krasnoperov V, Gill PS, and Duarte A**. Combination of Dll4/Notch and Ephrin-B2/EphB4 targeted therapy is highly effective in disrupting tumor angiogenesis. *BMC Cancer* 10: 641, 2010.
14. **Ehling M, Adams S, Benedito R, and Adams RH**. Notch controls retinal blood vessel maturation and quiescence. *Development* 140: 3051-3061, 2013.

15. **Erickson KK, Sundstrom JM, and Antonetti DA**. Vascular permeability in ocular disease and the role of tight junctions. *Angiogenesis* 10: 103-117, 2007.
16. **Fabian KP, Chi-Sabins N, Taylor JL, Fecek R, Weinstein A, and Storkus WJ**. Therapeutic efficacy of combined vaccination against tumor pericyte-associated antigens DLK1 and DLK2 in mice. *Oncoimmunology* 6: e1290035, 2017.
17. **Frye M, Dierkes M, Kuppers V, Vockel M, Tomm J, Zeuschner D, Rossaint J, Zarbock A, Koh GY, Peters K, Nottebaum AF, and Vestweber D**. Interfering with VE-PTP stabilizes endothelial junctions in vivo via Tie-2 in the absence of VE-cadherin. *J Exp Med* 212: 2267-2287, 2015.
18. **Fukumura D, Duda DG, Munn LL, and Jain RK**. Tumor microvasculature and microenvironment: novel insights through intravital imaging in pre-clinical models. *Microcirculation* 17: 206-225, 2010.
19. **Harrington LS, Sainson RC, Williams CK, Taylor JM, Shi W, Li JL, and Harris AL**. Regulation of multiple angiogenic pathways by Dll4 and Notch in human umbilical vein endothelial cells. *Microvasc Res* 75: 144-154, 2008.
20. **Hellstrom M, Phng LK, Hofmann JJ, Wallgard E, Coultas L, Lindblom P, Alva J, Nilsson AK, Karlsson L, Gaiano N, Yoon K, Rossant J, Iruela-Arispe ML, Kalen M, Gerhardt H, and Betsholtz C**. Dll4 signalling through Notch1 regulates formation of tip cells during angiogenesis. *Nature* 445: 776-780, 2007.
21. **Jakobsson L, Franco CA, Bentley K, Collins RT, Ponsioen B, Aspalter IM, Rosewell I, Busse M, Thurston G, Medvinsky A, Schulte-Merker S, and Gerhardt H**. Endothelial cells dynamically compete for the tip cell position during angiogenic sprouting. *Nat Cell Biol* 12: 943-953, 2010.
22. **Jayson GC, Zweit J, Jackson A, Mulatero C, Julyan P, Ranson M, Broughton L, Wagstaff J, Hakannson L, Groenewegen G, Bailey J, Smith N, Hastings D, Lawrance J, Haroon H, Ward T, McGown AT, Tang M, Levitt D, Marreaud S, Lehmann FF, Herold M, Zwierzina H, European Organisation for R, and Treatment of Cancer Biological Therapeutic Development G**. Molecular imaging and biological evaluation of HuMV833 anti-VEGF antibody: implications for trial design of antiangiogenic antibodies. *J Natl Cancer Inst* 94: 1484-1493, 2002.
23. **Jones EA, Yuan L, Breant C, Watts RJ, and Eichmann A**. Separating genetic and hemodynamic defects in neuropilin 1 knockout embryos. *Development* 135: 2479-2488, 2008.
24. **Kalen M, Heikura T, Karvinen H, Nitzsche A, Weber H, Esser N, Yla-Herttuala S, and Hellstrom M**. Gamma-secretase inhibitor treatment promotes VEGF-A-driven blood vessel growth and vascular leakage but disrupts neovascular perfusion. *PLoS One* 6: e18709, 2011.
25. **Keck PJ, Hauser SD, Krivi G, Sanzo K, Warren T, Feder J, and Connolly DT**. Vascular permeability factor, an endothelial cell mitogen related to PDGF. *Science* 246: 1309-1312, 1989.
26. **Lichtenbeld HC, Ferarra N, Jain RK, and Munn LL**. Effect of local anti-VEGF antibody treatment on tumor microvessel permeability. *Microvasc Res* 57: 357-362, 1999.
27. **Liu ZJ, Shirakawa T, Li Y, Soma A, Oka M, Dotto GP, Fairman RM, Velazquez OC, and Herlyn M**. Regulation of Notch1 and Dll4 by vascular endothelial growth factor in arterial endothelial cells: implications for modulating arteriogenesis and angiogenesis. *Mol Cell Biol* 23: 14-25, 2003.

28. **Murata T, Ishibashi T, Khalil A, Hata Y, Yoshikawa H, and Inomata H**. Vascular endothelial growth factor plays a role in hyperpermeability of diabetic retinal vessels. *Ophthalmic Res* 27: 48-52, 1995.
29. **Ng AN, and Toresson H**. Gamma-secretase and metalloproteinase activity regulate the distribution of endoplasmic reticulum to hippocampal neuron dendritic spines. *Faseb J* 22: 2832-2842, 2008.
30. **Nieuwdorp M, van Haeften TW, Gouverneur MC, Mooij HL, van Lieshout MH, Levi M, Meijers JC, Holleman F, Hoekstra JB, Vink H, Kastelein JJ, and Stroes ES**. Loss of endothelial glycocalyx during acute hyperglycemia coincides with endothelial dysfunction and coagulation activation in vivo. *Diabetes* 55: 480-486, 2006.
31. **Noguera-Troise I, Daly C, Papadopoulos NJ, Coetzee S, Boland P, Gale NW, Lin HC, Yancopoulos GD, and Thurston G**. Blockade of Dll4 inhibits tumour growth by promoting non-productive angiogenesis. *Nature* 444: 1032-1037, 2006.
32. **Patel NS, Li JL, Generali D, Poulsom R, Cranston DW, and Harris AL**. Up-regulation of delta-like 4 ligand in human tumor vasculature and the role of basal expression in endothelial cell function. *Cancer Res* 65: 8690-8697, 2005.
33. **Polacheck WJ, Kutys ML, Yang J, Eyckmans J, Wu Y, Vasavada H, Hirschi KK, and Chen CS**. A non-canonical Notch complex regulates adherens junctions and vascular barrier function. *Nature* 2017.
34. **Qiao J, Huang F, and Lum H**. PKA inhibits RhoA activation: a protection mechanism against endothelial barrier dysfunction. *Am J Physiol Lung Cell Mol Physiol* 284: L972-980, 2003.
35. **Qin WD, Zhang F, Qin XJ, Wang J, Meng X, Wang H, Guo HP, Wu QZ, Wu DW, and Zhang MX**. Notch1 inhibition reduces low shear stress-induced plaque formation. *Int J Biochem Cell Biol* 72: 63-72, 2016.
36. **Radeva MY, Kugelmann D, Spindler V, and Waschke J**. PKA compartmentalization via AKAP220 and AKAP12 contributes to endothelial barrier regulation. *PLoS One* 9: e106733, 2014.
37. **Ridgway J, Zhang G, Wu Y, Stawicki S, Liang WC, Chanthery Y, Kowalski J, Watts RJ, Callahan C, Kasman I, Singh M, Chien M, Tan C, Hongo JA, de Sauvage F, Plowman G, and Yan M**. Inhibition of Dll4 signalling inhibits tumour growth by deregulating angiogenesis. *Nature* 444: 1083-1087, 2006.
38. **Rosenfeld PJ, Brown DM, Heier JS, Boyer DS, Kaiser PK, Chung CY, and Kim RY**. Ranibizumab for neovascular age-related macular degeneration. *N Engl J Med* 355: 1419-1431, 2006.
39. **Salmon AH, Neal CR, Sage LM, Glass CA, Harper SJ, and Bates DO**. Angiopoietin-1 alters microvascular permeability coefficients in vivo via modification of endothelial glycocalyx. *Cardiovasc Res* 83: 24-33, 2009.
40. **Senger DR, Galli SJ, Dvorak AM, Perruzzi CA, Harvey VS, and Dvorak HF**. Tumour Cells Secrete a Vascular Permeability Factor that Promotes Accumulation of Ascites Fluid. *Science* 219: 983-985, 1983.
41. **Suchting S, Freitas C, le Noble F, Benedito R, Breant C, Duarte A, and Eichmann A**. The Notch ligand Delta-like 4 negatively regulates endothelial tip cell formation and vessel branching. *Proc Natl Acad Sci U S A* 2007.
42. **Tzima E, Irani-Tehrani M, Kiosses WB, Dejana E, Schultz DA, Engelhardt B, Cao G, DeLisser H, and Schwartz MA**. A mechanosensory complex that mediates the endothelial cell response to fluid shear stress. *Nature* 437: 426-431, 2005.

43. **Waschke J, Drenckhahn D, Adamson RH, Barth H, and Curry FE**. cAMP protects endothelial barrier functions by preventing Rac-1 inhibition. *Am J Physiol Heart & Circ* 287: H2427-2433, 2004.
44. **Wood JM, Bold G, Buchdunger E, Cozens R, Ferrari S, Frei J, Hofmann F, Mestan J, Mett H, O'Reilly T, Persohn E, Rosel J, Schnell C, Stover D, Theuer A, Towbin H, Wenger F, Woods-Cook K, Menrad A, Siemeister G, Schirner M, Thierauch KH, Schneider MR, Drevs J, Martiny-Baron G, and Totzke F**. PTK787/ZK 222584, a novel and potent inhibitor of vascular endothelial growth factor receptor tyrosine kinases, impairs vascular endothelial growth factor-induced responses and tumor growth after oral administration. *Cancer Res* 60: 2178-2189, 2000.
45. **Wysolmerski RB, and Lagunoff D**. Regulation of permeabilized endothelial cell retraction by myosin phosphorylation. *Am J Physiol* 261: C32-40, 1991.
46. **Yoo CB, Yun SM, Jo C, and Koh YH**. gamma-Secretase-dependent cleavage of E-cadherin by staurosporine in breast cancer cells. *Cell Commun Adhes* 19: 11-16, 2012.
47. **Zhang GS, Tian Y, Huang JY, Tao RR, Liao MH, Lu YM, Ye WF, Wang R, Fukunaga K, Lou YJ, and Han F**. The gamma-secretase blocker DAPT reduces the permeability of the blood-brain barrier by decreasing the ubiquitination and degradation of occludin during permanent brain ischemia. *CNS Neurosci Ther* 19: 53-60, 2013.

Figure 1

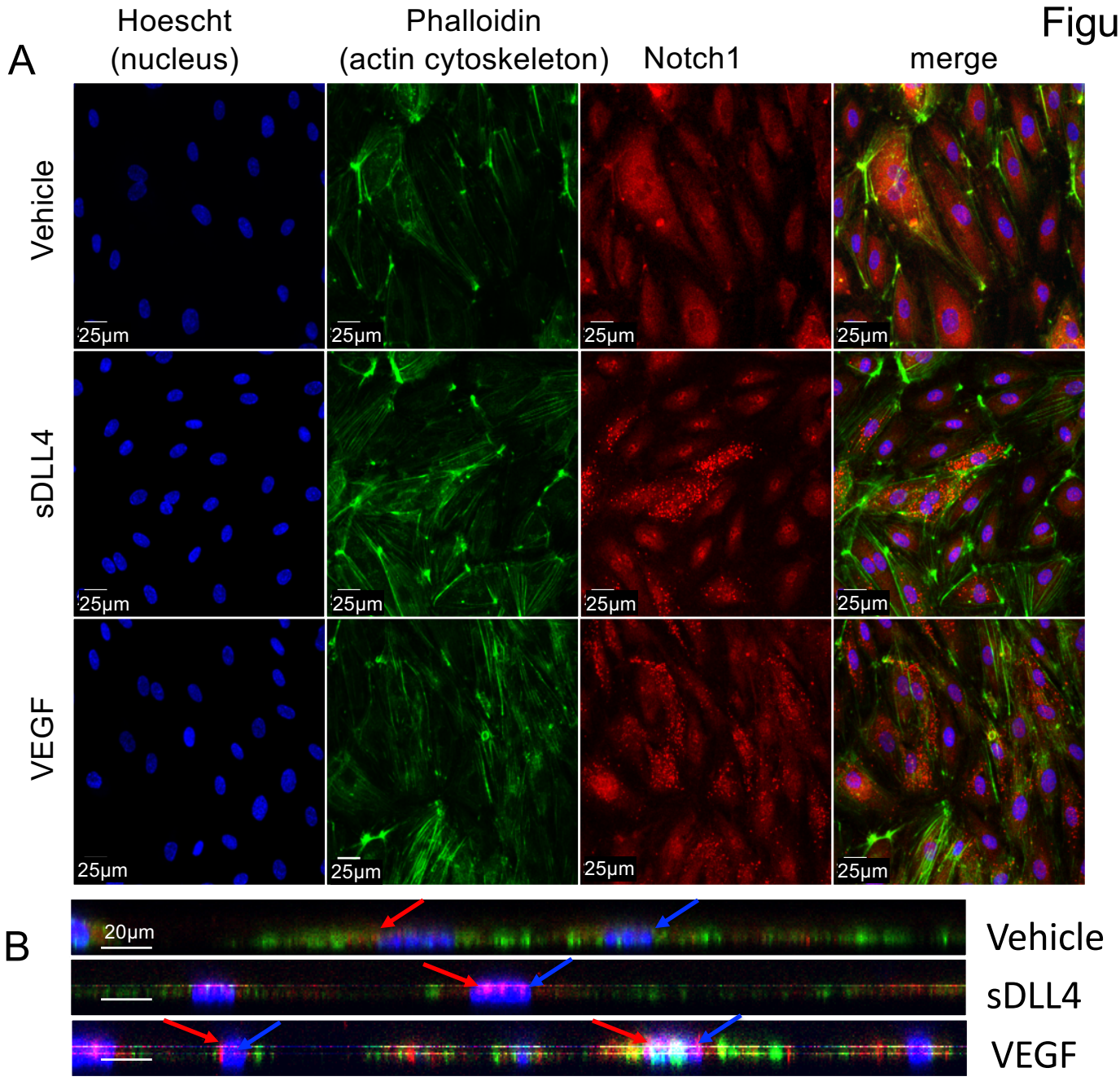
A
Hoescht (nucleus)
Phalloidin (actin cytoskeleton)
Notch1
merge
Vehicle
sDLL4
VEGF
25μm
B
20μm
Vehicle
sDLL4
VEGF

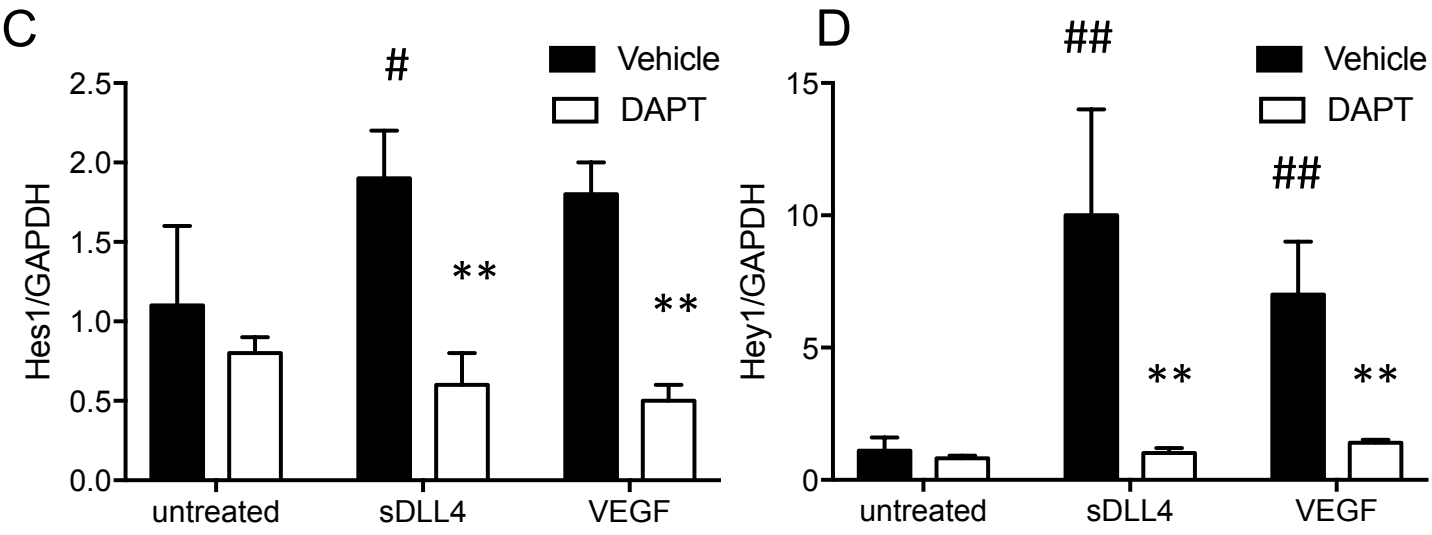
C
Hes1/GAPDH
2.5
2.0
1.5
1.0
0.5
0.0
#
**
**
Vehicle
DAPT
untreated
sDLL4
VEGF
D
Hey1/GAPDH
15
10
5
0
##
**
##
**
Vehicle
DAPT
untreated
sDLL4
VEGF

Figure 2

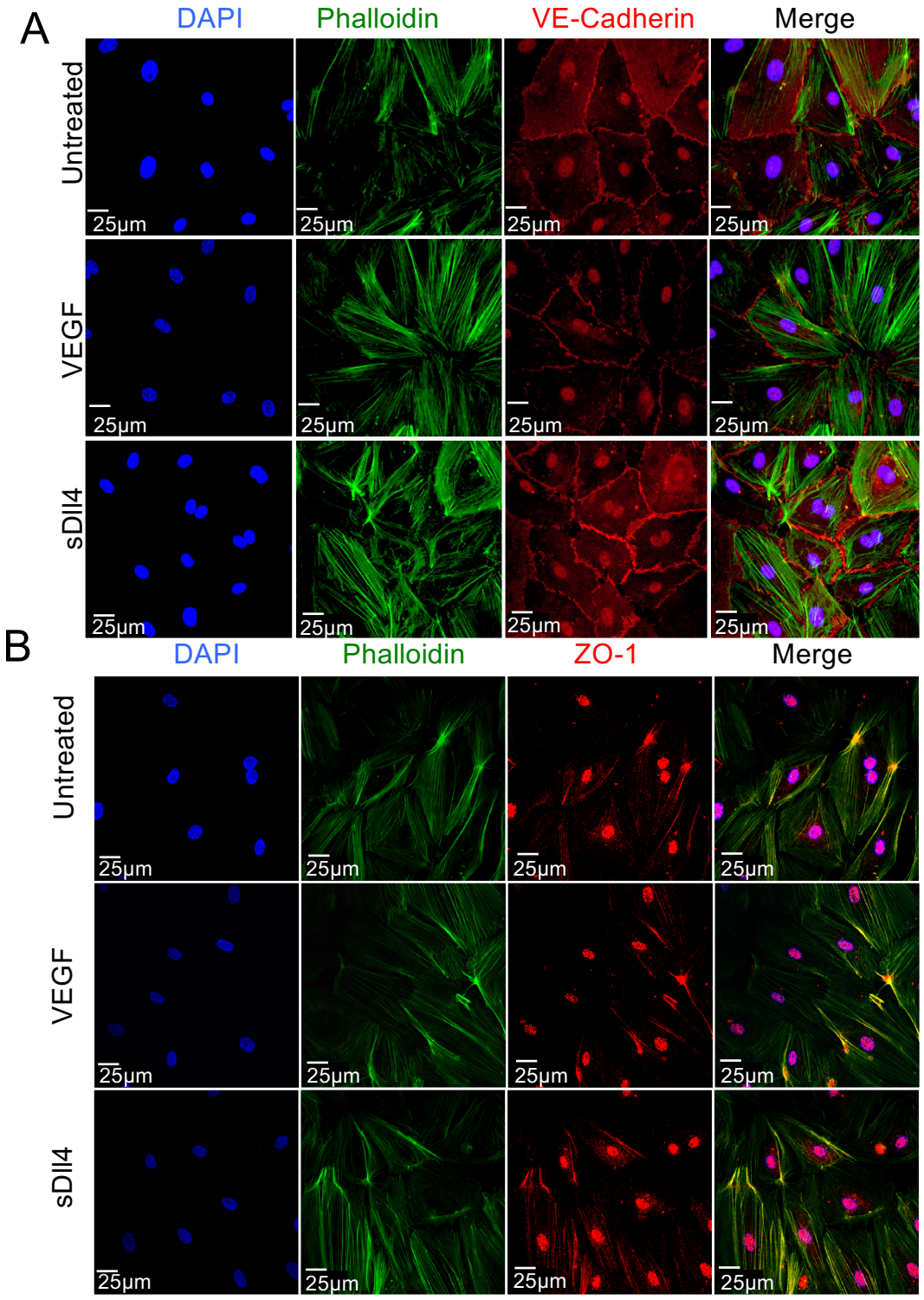
A
DAPI
Phalloidin
VE-Cadherin
Merge
Untreated
VEGF
sDll4
25μm
B
DAPI
Phalloidin
ZO-1
Merge
Untreated
VEGF
sDll4
25μm
C
Percentage of VE-Cad stained junctions (%)
80
60
40
20
0
**
****
***
Gaps
Thin Junction
Thick Junction
Untreated
VEGF
sDll4
D
Number of ZO1 Junctions / Cell
0.8
0.6
0.4
0.2
0.0
*
Untreated
sDll4
VEGF

Figure 3

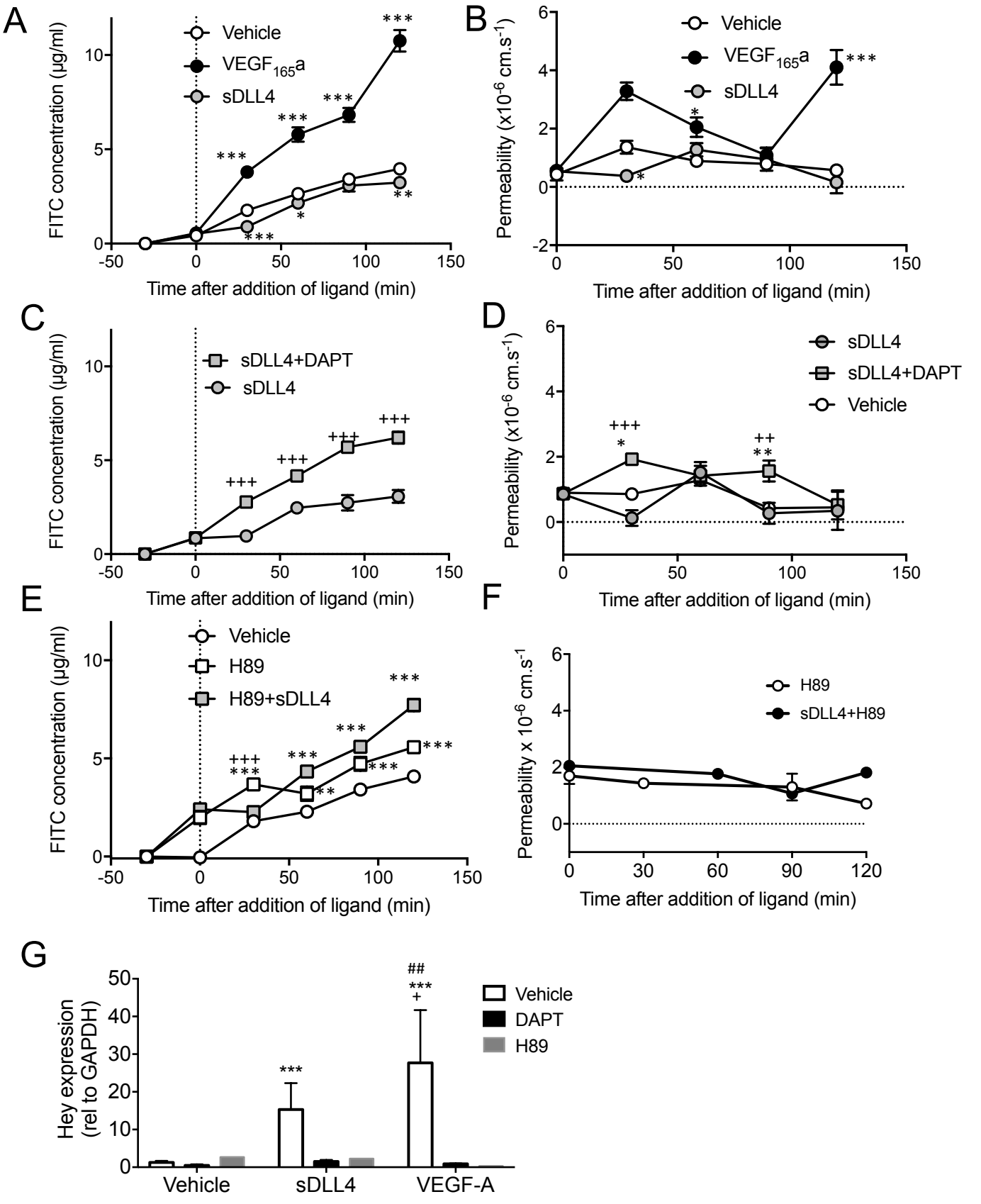
A
FITC concentration (µg/ml)
Time after addition of ligand (min)
Vehicle
VEGF165a
sDLL4
B
Permeability (x10-6 cm.s-1)
Time after addition of ligand (min)
Vehicle
VEGF165a
sDLL4
C
FITC concentration (µg/ml)
Time after addition of ligand (min)
sDLL4+DAPT
sDLL4
D
Permeability (x10-6 cm.s-1)
Time after addition of ligand (min)
sDLL4
sDLL4+DAPT
Vehicle
E
FITC concentration (µg/ml)
Time after addition of ligand (min)
Vehicle
H89
H89+sDLL4
F
Permeability x 10-6 cm.s-1
Time after addition of ligand (min)
H89
sDLL4+H89
G
Hey expression (rel to GAPDH)
Vehicle
sDLL4
VEGF-A
Vehicle
DAPT
H89

Figure 4

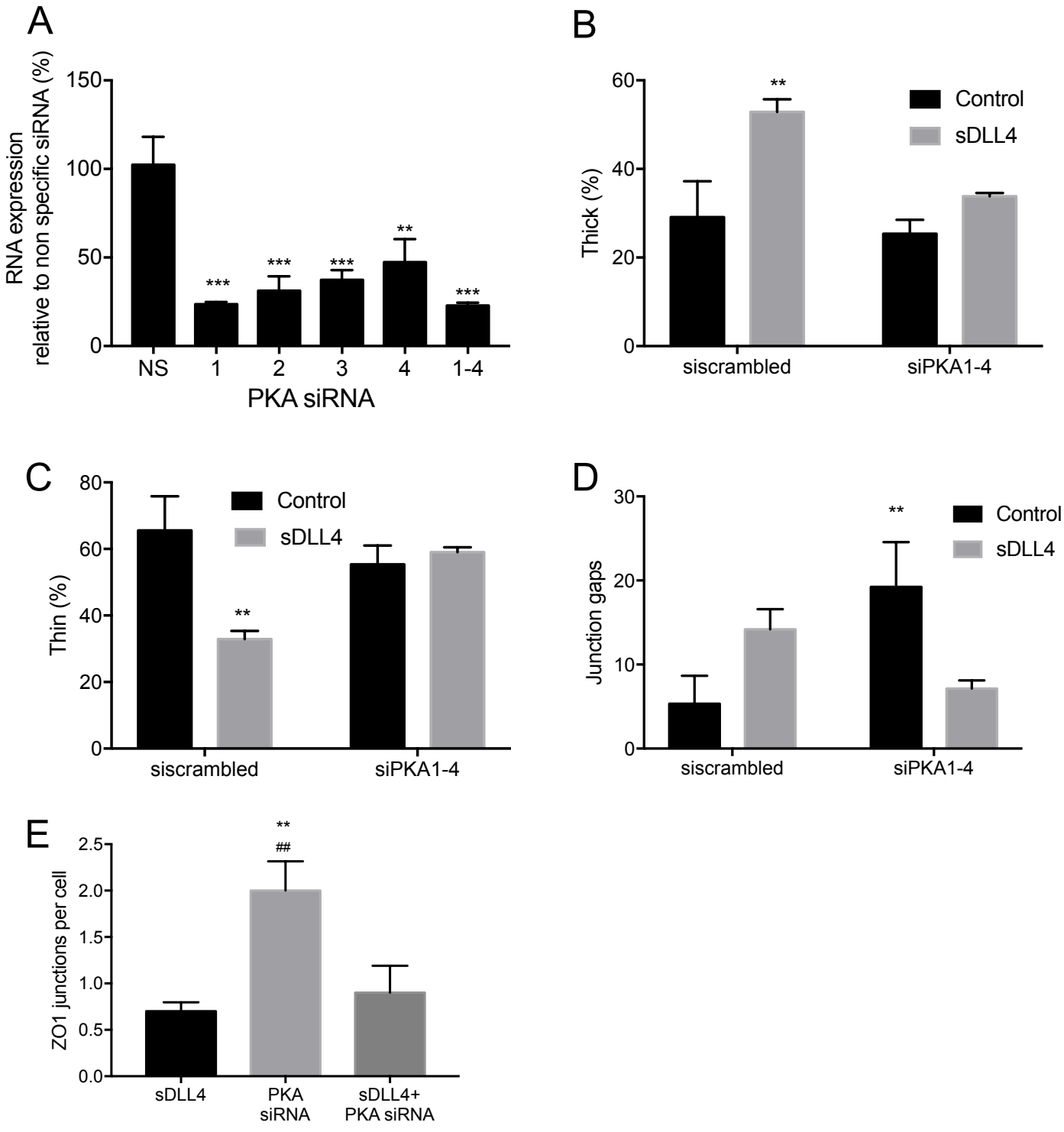
A
RNA expression relative to non specific siRNA (%)
150
100
50
0
***
***
***
**
***
NS
1
2
3
4
1-4
PKA siRNA
B
Thick (%)
60
40
20
0
**
Control
sDLL4
siscrambled
siPKA1-4
C
Thin (%)
80
60
40
20
0
Control
sDLL4
**
siscrambled
siPKA1-4
D
Junction gaps
30
20
10
0
**
Control
sDLL4
siscrambled
siPKA1-4
E
ZO1 junctions per cell
2.5
2.0
1.5
1.0
0.5
0.0
**
##
sDLL4
PKA siRNA
sDLL4+ PKA siRNA

Figure 5

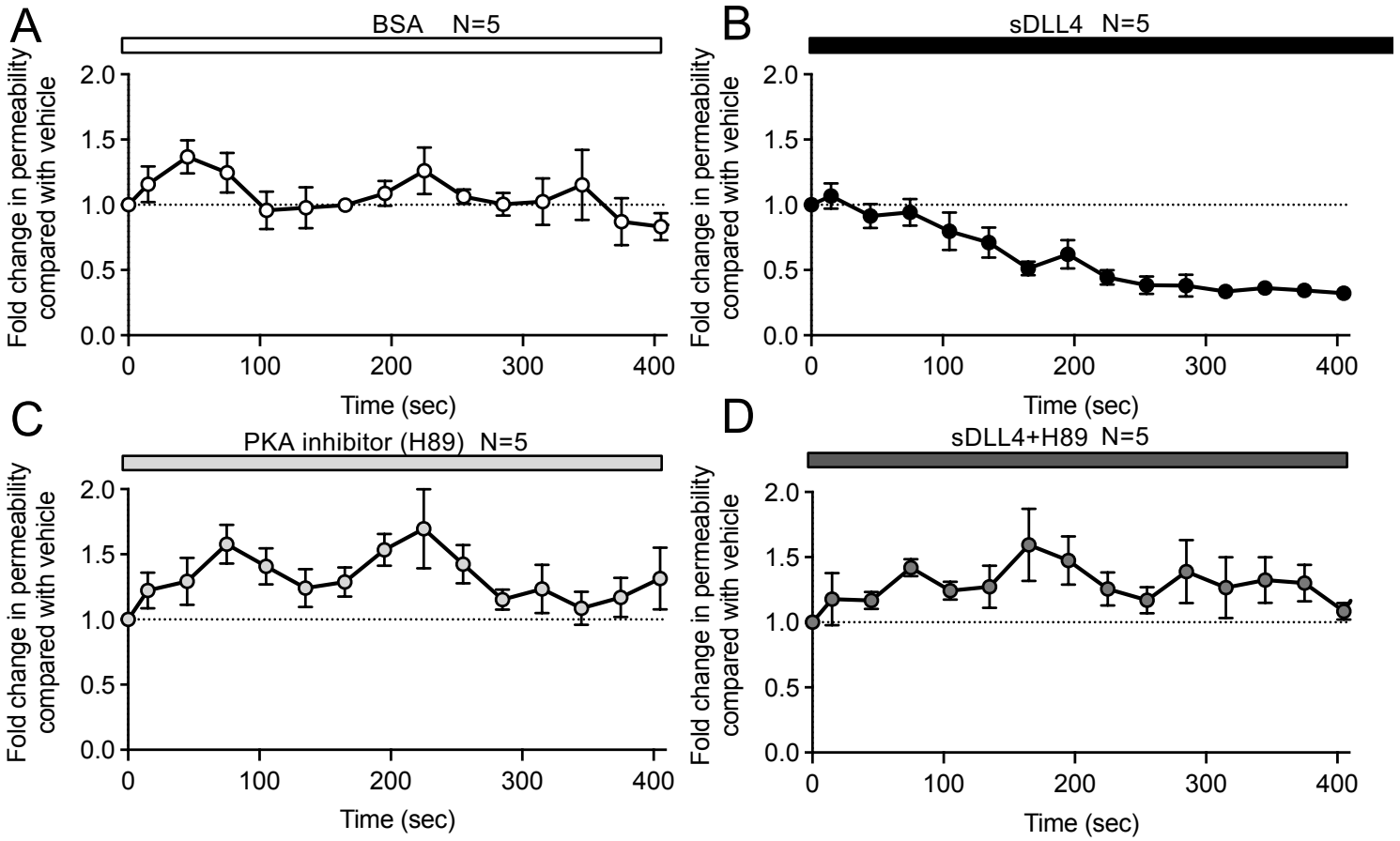
A
BSA N=5
B
sDLL4 N=5
C
PKA inhibitor (H89) N=5
D
sDLL4+H89 N=5
Fold change in permeability compared with vehicle
Time (sec)
0.0
0.5
1.0
1.5
2.0
0
100
200
300
400

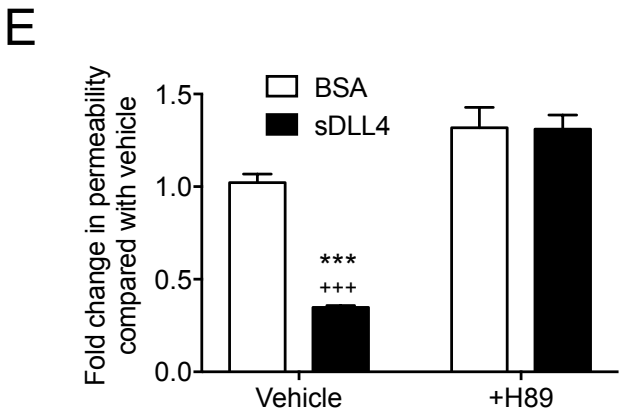
E
BSA
sDLL4
Fold change in permeability compared with vehicle
0.0
0.5
1.0
1.5
***
+++
Vehicle
+H89

Figure 6

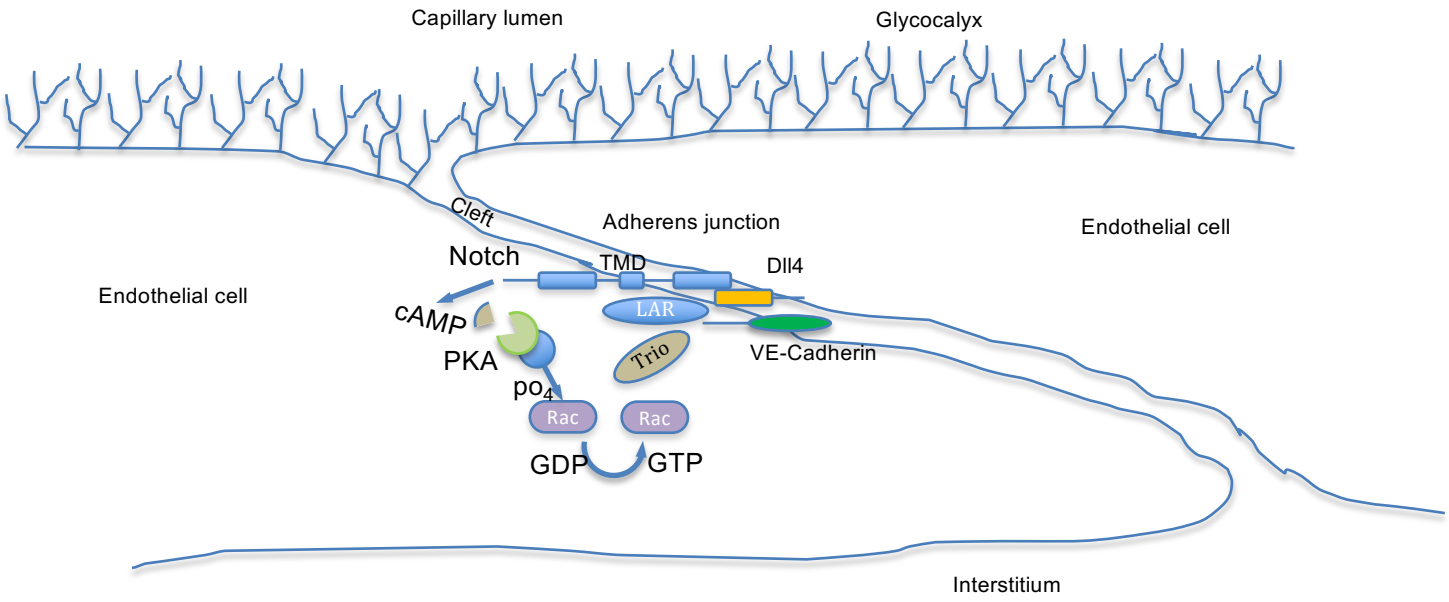
Capillary lumen
Glycocalyx
Cleft
Adherens junction
Endothelial cell
Endothelial cell
Notch
TMD
Dll4
cAMP
LAR
PKA
Trio
VE-Cadherin
po4
Rac
Rac
GDP
GTP
Interstitium